Current Research in Food Science 9 (2024) 100814

Contents lists available at ScienceDirect

Current Research in Food Science

journal homepage: www.sciencedirect.com/journal/current-research-in-food-science

Enhancement of the gelling properties of *Aristichthys nobilis*: Insights into intermolecular interactions between okra polysaccharide and myofibrillar protein

Xin Wang [a,1], Mengzhe Li [a,1], Tong Shi [a,**], Abdul Razak Monto [a], Li Yuan [a], Wengang Jin [b], Ruichang Gao [a,b,*]

[a] School of Food and Biological Engineering, Jiangsu University, Zhenjiang, Jiangsu Province, 212013, China
[b] Bio-resources Key Laboratory of Shaanxi Province, School of Biological Science and Engineering, Shaanxi University of Technology, Hanzhong, 723001, China

ARTICLE INFO

Handling editor: Dr. Quancai Sun

Keywords:
Okra polysaccharide
Myofibrillar proteins
Gel properties
Molecular interaction
Microstructure

ABSTRACT

The effects of various contents of okra polysaccharide (OP) (0%–1%) on myofibrillar protein (MP) gelation and the interaction mechanism between OP and MP were investigated. OP improved the gelling properties of MP with an additive limitation of 0.75%. Rheological analysis demonstrated that the addition of OP enhanced the interactions between MPs, resulting in a denser intermolecular gel network structure. The addition of OP shifted the I_{850}/I_{830} of Fourier transform infrared spectroscopy, indicating that hydrogen bonds were formed between OP and MP. Adding OP promoted the transition from α-helix to β-sheet in the MP. OP exposed the hydrophobic groups of MPs and increased the number of hydrophobic interactions between them, favoring the formation of a dense gel network. Molecular docking predicted that hydrogen bonds were the main force involved in the binding of OP and MP. Moderate OP promoted the aggregation of MPs and improved their functional properties, facilitating heat-induced gelation.

1. Introduction

Due to their high protein content, low fat content, and distinctive flavor, surimi products are well liked by consumers and manufacturers (Mi et al., 2022). The gel properties of the myofibrillar proteins (MPs) in surimi are the basis of the structural qualities, textural properties, appearance, and yield of surimi products (Zhu et al., 2022). As the protein gelling properties of freshwater surimi are less than those of sea fish surimi, food additives such as polysaccharides are added to surimi to produce high-quality protein-based surimi products (Zhang et al., 2023).

Polysaccharides, as hydrocolloids, have a positive effect on the quality of gel products due to their unique structure and function (Pirsa and Hafezi, 2023; Zhou et al., 2021). Moreover, functional polysaccharides can improve the nutritional value of products and have the potential to be used as fat substitutes to reduce fat content (Han et al., 2022). In the last few years, the application of different polysaccharides in MP gels has been extensively studied, and some have been successfully applied to freshwater fish surimi products, including konjac glucomannan, inulin, hsian-tsao polysaccharide and psyllium husk powder (Zhu et al., 2022; Zhuang et al., 2021; Han et al., 2022; You et al., 2023). The complex system formed by the interaction between polysaccharides and proteins can usually effectively adjust the gel properties, change the molecular structure, and produce products with better gelation properties and conformational stability (Gao et al., 2022). The structural characteristics of proteins and polysaccharides affect the formation and properties of hybrid gels, with the monosaccharide composition of polysaccharides being an important factor (Le et al., 2017). Polysaccharides contain a large number of active groups, such as hydroxyl, carboxyl and aldehyde groups, providing the possibility of interactions with protein molecules (Nagae and Yamaguchi, 2014). For example, the monosaccharides with high contents in hsian-tsao polysaccharide and psyllium husk powder are all polyhydroxy monosaccharides, which promote polysaccharide interactions with proteins through hydroxyl groups (Zhuang et al., 2021; Han et al., 2022; You et al., 2023; Gonzalez et al., 2019; Le et al., 2017; Nagae and Yamaguchi, 2014; Zhang et al., 2020). Although the mechanism

* Corresponding author. School of Food and Biological Engineering, Jiangsu University, No.301, Xuefu Road, Zhenjiang, Jiangsu Province, 212013, China.
** Corresponding author.
E-mail addresses: 1000005720@ujs.edu.cn (T. Shi), xiyuan2008@ujs.edu.cn (R. Gao).
[1] These authors contributed equally to this work.

https://doi.org/10.1016/j.crfs.2024.100814
Received 19 June 2024; Received in revised form 8 July 2024; Accepted 20 July 2024
Available online 21 July 2024

underlying the effect of polysaccharides on surimi has been partially explained, few studies have explored the interactions between polysaccharides and proteins by focusing on the types of monosaccharides in polysaccharides and the molecular structure characteristics of polysaccharides or have then investigated the effect of polysaccharides on the structural characteristics of proteins.

Abelmoschus esculentus L. (okra), a member of the Malva family, provides a good dietary source of fibers and bioactive substances and contains pectin polysaccharides that are particularly suitable for applications in food (Alba et al., 2021). Okra polysaccharide (OP), an anionic polysaccharide, has been verified to consist mainly of galactose and rhamnose at molar ratios of 18.3 and 5.5, respectively, with uncommon terminal α-Galp and acetylation of Rhap residues (Olawuyi and Lee, 2021). The structure of OP is different from that of other acetylated pectin polysaccharides that have acetyl groups attached exclusively to GalpA residues (Alba et al., 2021). OP is currently used as a viscosity enhancer, gelling agent, and texture modifier in food (Zhuang et al., 2021). Recent studies have shown that OP can be added to yogurt and ice cream as fat substitutes and improve the texture and taste of food (Xu et al., 2019a; Yuennan et al., 2014). However, few studies have examined the addition of OP to freshwater fish surimi and explored the effect of OP on MP structure and the interaction mechanism between OP and MP, especially the role of monosaccharides (galactose/rhamnose) in the polysaccharides.

In this work, OP was added to MP to alter the physical properties of MP gels. The effects of OP on MP gel properties were measured by gel strength, rheological properties, and microstructure. Changes in the functional groups, secondary structures, and tertiary structures of the composite system were examined to elucidate the mechanism underlying the influence of polysaccharides on protein structure. Furthermore, molecular docking was performed to confirm the interactions between OP and MP. This work offered a theoretical foundation for using OP in surimi products.

2. Materials and methods

2.1. Materials and chemicals

Fresh bighead carp (*Aristichthys nobilis*) weighing 1.7 ± 0.5 kg were purchased from the Jimailong supermarket in Zhenjiang, Jiangsu Province, China. OP with a polysaccharide content of 75% was purchased from Baoyifeng Biotechnology Co., Ltd. (Shaanxi, China). The moisture, crude protein, polyphenol, and ash contents of the OP sample were determined to be 8.04%, 0.84%, 1.66%, and 8.61%, respectively. All the analytical grade chemicals used were obtained from Sinopharm Chemical Reagent Co., Ltd. (Shanghai, China).

2.2. Extraction of MP

The MP was obtained by slightly altering a previous method (Cao et al., 2021). The minced nonspiky bighead carp muscle was centrifuged (10,000×*g*, 15 min, 4 °C, CR21N, Eppendorf Himac Technologies Co., Japan) with 5 vol (w/v) of 0.02 mol/L cold Tris-HCl containing 0.1 mol/L NaCl (pH 7.0) three times. The precipitate was centrifuged with 5 vol (w/v) of 0.02 mol/L cold Tris-HCl containing 0.6 mol/L NaCl (pH 7.0) under the same conditions to collect the supernatant as MP. The MP was kept at 4 °C for the next experiment for no more than 2 days.

2.3. Preparation of OP–MP composite solutions and gels

The approach of Zhang et al. (2020) was used to create complicated solutions and gels for OP-MP. Five different contents of OP was added to MP solutions (25 mg/mL): 0 (control group), 0.25, 0.5, 0.75, and 1 g/100 g MP (0, 0.25% 0.5% 0.75%, and 1%). After stirring the OP-MP solutions for 30 min to ensure that the OP was distributed evenly, the bubbles were eliminated by centrifuging the mixtures at 4 °C for 5 min at 1000 r/min. The OP-MP solutions were heated in two different ways: (i) Stage A: MP solutions were not heated; (ii) Stage B: MP solutions were heated at 40 °C for 60 min and then heated at 90 °C for 30 min. The heated samples were put in a 4 °C refrigerator after a quick cooling process in ice water.

2.4. Turbidity determination

With slight adjustments, the turbidity was determined using the method described by Shi et al. (2019). OP-MP solutions (0.5 mg/mL) were heated under Stages A and B. A UV/visible spectrophotometer (UV, 1910, Shanghai Lingguang Technology Co., Ltd., Shanghai, China) was used to measure the absorbance of the samples at 340 nm to determine protein turbidity.

2.5. Particle size

Following Stage A and B processing, the particle sizes of the OP–MP complex samples (MP, 10 mg/mL) were assessed using a Mastersizer 3000 laser particle size analyzer (MS 3000, Malvern Instruments Limited Co., Ltd., Malvern, U.K.), in accordance with the method described by Ma et al. (2022). The dispersant had a refractive index of 1.330 and a refractive index of 1.434.

2.6. Gel strength, water holding capacity (WHC), and cooking yield

The previous method was modified somewhat for the purpose of measuring the gel strength of the OP-MP gels (Li et al., 2022). Following Stage B, the samples (15 mm in diameter and 40 mm in height) underwent a puncture test using a P/5 probe and a TAXT Plus texture analyzer (Stable Micro Systems Co., Ltd., Surrey, UK). The following test parameters were used: distance of 5 mm, trigger force of 2.0 g, pretest speed of 2.0 mm/s, test speed of 2.0 mm/s, and posttest speed of 4.0 mm/s. Five parallel tests were performed on each group of samples. The formula for calculating gel strength was as follows:

$$Gel\ strength(g \bullet mm) = Breaking\ force(g) \times Deformation(mm)$$

The WHC was calculated using the centrifugal method (Shi et al., 2022). After Stage B, 3.0 g of OP–MP gels were centrifuged at 10,000×*g* for 5 min at 4 °C. The following equation described the WHC:

$$WHC(\%) = M_b/M_a \times 100$$

M_a was the weight of the gel before centrifugation, and M_b was the weight of the gel after centrifugation.

The cooking yield was tested according to Han et al. (2022). The cooking yield is the weight ratio of the heat-induced gel to the original MP solution after eliminating all the liquid that separated from the gel. The cooking yield was calculated using the following equation:

$$Cooking\ yield\ (\%) = M_d/M_c \times 100$$

M_c was the weight of the unheated MP solution, and M_d was the weight of the heat-induced MP gel.

2.7. Dynamic rheological analysis

OP-MP composites were subjected to dynamic rheological experiments on a rheometer (Discovery HR-1, TA Instruments Co., Ltd., New Castle DE, USA) by Zhu et al. (2022) with various modifications. The samples were heated at a rate of 2 °C/min from 20 °C to 90 °C and then cooled at a rate of 5 °C/min to 20 °C. Automatic recording of the G′ values was performed throughout the temperature fluctuations.

2.8. Intermolecular forces

With small adjustments, the method of Zhu et al. (2022) for

determining gel solubility was used to examine the intermolecular forces of OP-MP gels. The gels were dissolved in turn using S_1 (0.05 mol/L NaCl), S_2 (0.6 mol/L NaCl), S_3 (0.6 mol/L NaCl and 1.5 mol/L urea), S_4 (0.6 mol/L NaCl and 8 mol/L urea), and S_5 (0.6 mol/L NaCl, 8 mol/L urea, and 0.5 mol/L β-mercaptoethanol). Using a T25 Ultra-Turrax homogenizer (IKA Labortechnik, Staufen, Germany), 2.0 g OP-MP gel samples were homogenized at 10,000 r/min with 10 mL of each solution. At 4 °C, the sample was centrifuged at 10,000×*g* for 15 min after being mixed for 1 h. By comparing the protein content of each solution, the intermolecular forces were measured and quantified. The differences in protein content between the S_2 and S_1, S_3 and S_2, S_4 and S_3, and S_5 and S_4 solutions represented the contributions of ionic bonds, hydrogen bonds, hydrophobic interactions, and disulfide bonds, respectively. The data are presented as mg soluble protein/mL of homogenate.

2.9. Fourier transform infrared (FTIR) spectroscopy

The OP, MP and OP-MP composite samples were mixed with KBr at a ratio of 3:100. The mixed powder was pressed into a sheet by applying 15 tons of pressure for 1 min. The samples were analyzed by a Nicolet 50 Fourier transform infrared (FTIR) spectrophotometer (Nicolet Co., Ltd., Madison, USA) according to Fan et al. (2017). The spectral range was 500–4000 cm^{-1}, and the spectral resolution was 4 cm^{-1}.

2.10. Far-UV circular dichroism (CD) spectroscopy

Using a Jasco J-815 spectropolarimeter (Jasco Co., Ltd., Tokyo, Japan), CD spectra of OP-MP (0.1 mg/mL) solutions were acquired according to the method described by Shi et al. (2021). The samples subjected to Stages A and B were scanned at a scan rate of 100 nm/min from 200 nm to 260 nm. The protein secondary structure was calculated as the ratio of α-helix, β-sheet, β-turn, and random coil structures by CD Pro.

2.11. Intrinsic tryptophan fluorescence emission spectroscopy

OP-MP solutions (0.1 mg/mL) underwent Stage A and B treatment and then were scanned in a Cary Eclipse fluorescence spectrophotometer (Varian Co., Ltd., California, America) with modifications from Cao et al. (2021). The emission spectra were acquired in the 300–450 nm range, with the excitation wavelength set at 280 nm. The excitation slit width was set at 5 nm, and the emission slit width was the same.

2.12. Microstructure

2.12.1. Confocal laser scanning microscopy (CLSM)

According to the methods of Li et al. (2022), a Leica TCS SP5 confocal laser scanning microscope system (Leica Co., Ltd., Weztlar, Germany) was used to assess the distribution of the MP and OP. Fast Green (1.0 mg/mL, dissolved in ethanol) and Calcofluor White (1 mg/mL, dissolved in DMSO) were used to stain the MP and OP, respectively. The prepared samples (1.0 mL) that underwent Stage A and B treatment were first stained by mixing with 40 μL of Calcofluor White (1.0 mg/mL) and 40 μL of Fast Green (1.0 mg/mL) and then placed in the dark for 1 h. The samples were observed under a microscope at 40 × magnification, and the excitation was performed using two laser beams at 405 nm (for Calcofluor White) and 633 nm (for Fast Green).

2.12.2. Scanning electron microscopy (SEM)

MP gels were cut into 1 mm cubes, placed in 0.2 M phosphate buffer solution (pH 7.2) containing 2.5% glutaraldehyde for at least 3 h, and then dehydrated with gradient ethanol (Zhang et al., 2020). The evaporated samples were washed three times with tertiary butanol. Subsequently, the samples were desiccated in a freezing dryer (FD-1A-50, Biocool Co., Ltd., Beijing, China). The microstructure of the MP gel was viewed by scanning electron microscopy (SEM) (Quanta FEG 250, FEI Company, Hillsboro, USA) at 10,000 × magnification.

2.13. Molecular docking of myosin with galactose and rhamnose

According to the method of Mi et al. (2022) with some modifications, a molecular docking experiment between myosin and galactose/rhamnose was carried out to predict and analyze the interactions between MP and OP. The *Aristichthys nobilis* myosin heavy chain (MHC) was constructed with Discovery Studio 4.1 in Builder Homology Models as described by Shi et al. (2022). The 3D structures of galactose and rhamnose were acquired from the PubChem database (http://pubchem.ncbi.nlm.nih.gov/) and constructed as ligand structures. A docking process was used to attach the galactose/rhamnose ligand to the MHC receptor. The free binding energy of galactose/rhamnose to MHC was established using the MM/GBVI method.

2.14. Statistical analysis

The statistical analysis of variances, means, and standard errors was carried out using Excel 2017 (Microsoft Office Excel, 2017 for Windows). A significant ($P < 0.05$) difference analysis was performed using the SPSS 17.0 program (SPSS 17.0 for Windows, SPSS Inc., Chicago, IL, USA). One-way ANOVA and Tukey's test were utilized to evaluate significant differences, and graphs were created using Origin 8.0 (Origin Lab Co., Northampton, MA, USA).

3. Results and discussion

3.1. Effects of OP on the heat-induced aggregation of MPs

The degree of protein aggregation can be determined by turbidity and particle size variations in protein solutions (Shi et al., 2019; Ma et al., 2022). The impacts of the thermal treatments on the turbidity of the MP solutions containing various amounts of OP are shown in Fig. 1 (A). The turbidity of the MP treated with OP did not significantly ($P > 0.05$) differ from that of the control at Stage A but significantly ($P < 0.05$) increased after Stage B. The turbidity of the control rapidly ($P < 0.05$) increased from 0.07 to 0.29 after Stage B. The unfolding of the protein structure and the exposure of hydrophobic/sulfhydryl groups accelerate at temperatures above 40 °C, which promoted protein aggregation via hydrophobic interactions/covalent bonds (Cao et al., 2021). For the samples subjected to Stage B, the turbidity of the MP solutions reached the highest value of 0.46 when the additional amount of OP was 0.75%. The turbidity of OP was not affected by heating (Xu et al., 2019b); thus, the increase in turbidity in the composite system occurred because the presence of sufficient OP molecules promoted the denaturation and aggregation of MP.

The particle sizes of the MPs significantly ($P < 0.05$) changed with the addition of OP at Stage A. Differences in the turbidity and particle sizes of the MPs at Stage A might be related to differences in the contents of the MPs. As depicted in Fig. 1 (B), the peak MP particle sizes at Stage A were distributed near 10 μm and 100 μm. The percentage of large particles increased, whereas the proportion of small particles decreased with OP. In comparison, the particle size distribution exhibited an agglomeration peak on the right with a greater peak value (larger particle sizes) after the MP was subjected to Stage B (Fig. 1 (C)), suggesting that the temperature was positively correlated with the degree of MP aggregation. The particle sizes of the MPs with 0.75% and 1% OP were larger than those of the MPs with other OP amounts (0%–0.5%). The MP was more likely to develop a stable network structure with larger particle sizes (Zhu et al., 2022). Xu et al. (2019) reported that protein clusters of yogurt casein became larger with increasing contents of OP. According to these findings, OP weakened the repulsion between MPs and favored MP aggregation. The addition of polysaccharides with higher hydroxyl content to the protein may cause competition for water between the protein and the polysaccharide (Han et al., 2022). Based on

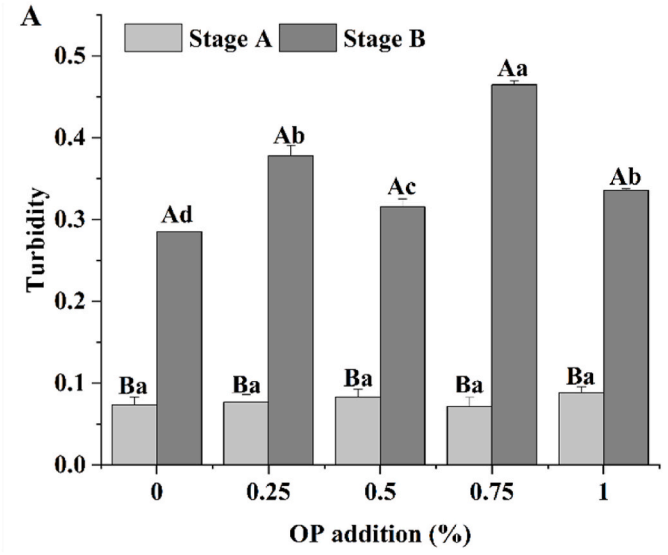

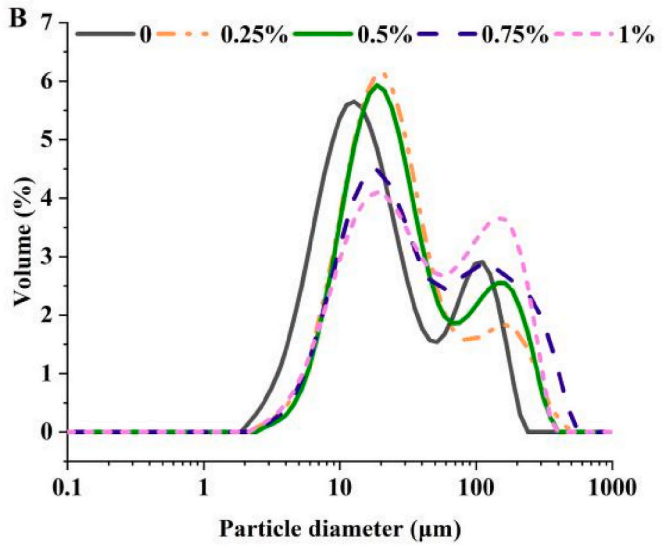

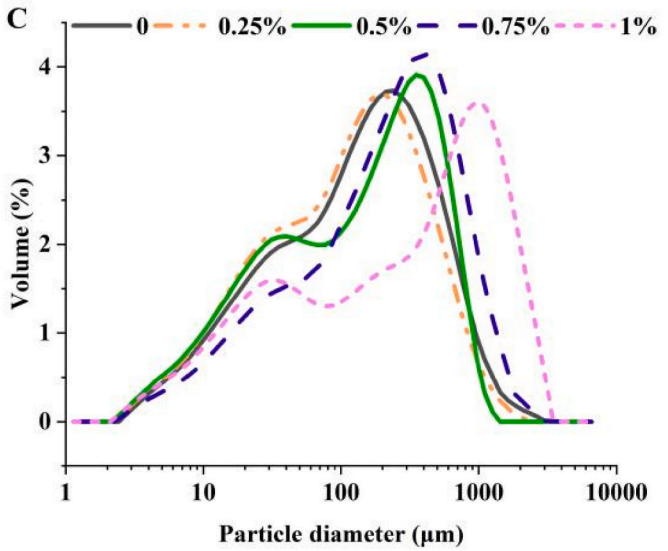

(caption on next column)

Fig. 1. Effects of OP addition (0%~1%) on the turbidity (A) and effects of OP addition on the particle size of MP treated with Stages A (B) and B (C) heating. Stage A, MP solutions without heating; Stage B, MP solutions heating at 40 °C for 1 h and 90 °C for 30 min. Different letters in the graph bars show significant ($P < 0.05$) differences, where lowercase letters (a–d) denote significance ($P < 0.05$) of different samples at the same heating treatment, and capital letters (A–B) denote significance ($P < 0.05$) of the same sample at different heating treatments.

the above results, it is speculated that OP molecules compete with water and cause an increase in protein aggregation.

3.2. Effects of OP on the gelling properties of MP

3.2.1. Gel strength

The gel strength of MP can be used to reflect the gel quality of protein in meat and meat products (Zhang et al., 2020). The gel strength of the control group in this experiment was 8.97 g × mm, which fell below the value of the control group reported by Li et al. (2022). The gel strength increased marginally with increasing OP addition and reached a maximum value 2.43 times (21.79 × mm) greater ($P < 0.05$) than that of the control group (8.97 × mm) when the addition amount of OP was 0.75% (Fig. 2 (A)). The combination of OP with a large number of water molecules through hydrogen bonds caused the formation of circular cavities inserted in the three-dimensional gel network of MP, which could also contribute to increasing the gel strength of the OP-MP gels (Sun et al., 2024). However, the excessive addition of OP to the MP gel network might prevent MP from cross-linking, thereby reducing the gel strength of the composite gel (Zhou et al., 2021).

3.2.2. WHC

A high WHC reveals that the surimi product has a strong three-dimensional network structure with a significant capacity to collect and retain water (Mi et al., 2022). The WHCs of the composite gels with different OP additions are shown in Fig. 2 (A). Compared to the WHC of the control group, that of the OP-MP gels considerably ($P < 0.05$) increased until the OP content exceeded 0.75%. The WHC of the gels increased significantly ($P < 0.05$) from 40.77% to 51.44% as the OP content increased from 0 to 1%. A significant amount of OP can readily dissolve in water at room temperature (Olawuyi and Lee, 2021), which reduces water movement in the matrix area and promotes hydration of the MP gel structure (Xu et al., 2019a), enhancing the WHC of the MP gel.

3.2.3. Cooking yield

During the heating phase, the cooking yield is crucial for determining the water-binding properties of myofibrillar proteins (Shi et al., 2022). As displayed in Fig. 2 (A), the cooking yield increased considerably ($P < 0.05$) with increasing OP content (0%~0.75%), but it decreased significantly ($P < 0.05$) with 1% OP. This result demonstrated that OP could prevent a fraction of moisture loss from MP gels. The reason for this enhancement is that hydroxyl groups in OP can increase the cooking yield of OP-MP gels by forming hydrogen bonds with water molecules inside the gel network (Sun et al., 2024). These results essentially coincided with the WHC and gel strength results (Fig. 2 (A)), revealing the clear effect of 0.75% OP on enhancing the gel properties of the MPs.

3.2.4. Rheological properties

The storage modulus (G′) represents the solid-like behavior of a material under deformation, which can reflect the viscoelastic properties of samples (Olawuyi and Lee, 2021; Li et al., 2022). The rheological characteristics of MP samples with various contents of OP are shown in Fig. 2 (B). The G′ values of the control group and OP-MP gels increased from 35 °C to a peak at 40 °C and then decreased to 46 °C before increasing steadily to 90 °C. The G′ of the OP-MP samples exhibited three similar and typical stages of heat-induced gelation of MP in the thermal

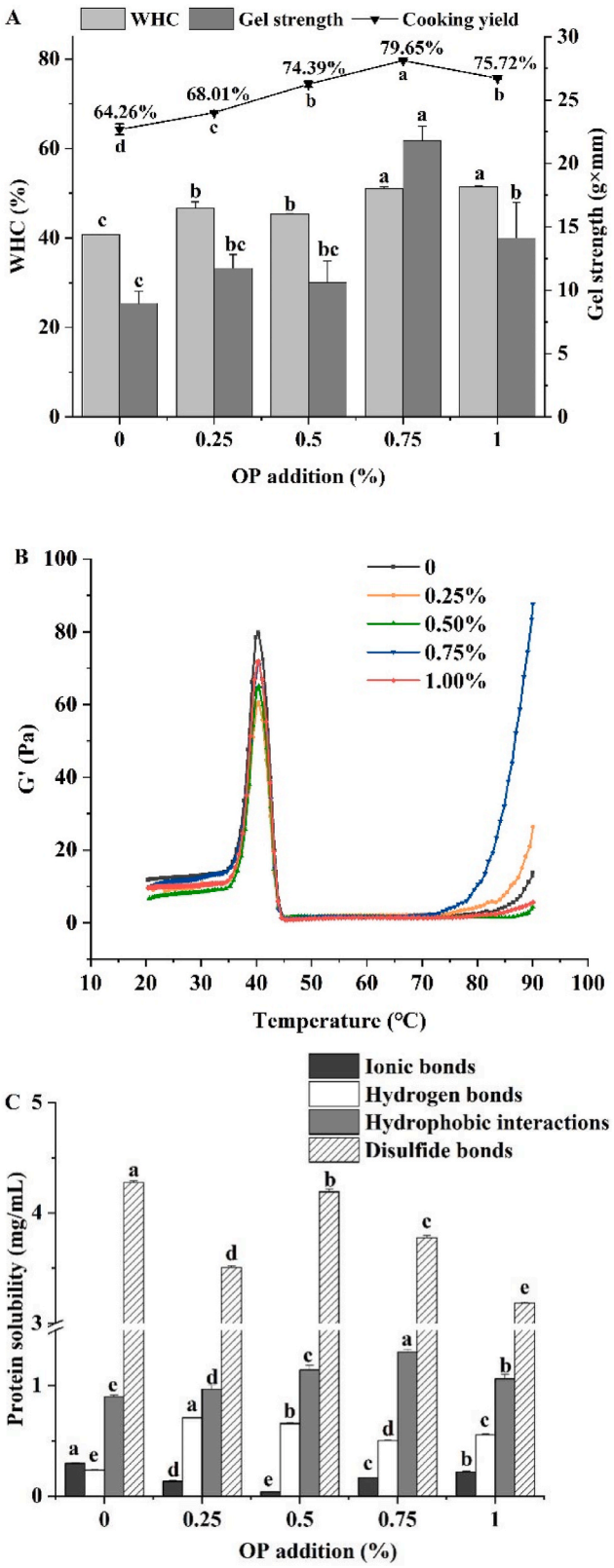

Fig. 2. Effects of OP addition (0%~1%) on WHC (A), gel strength (A) and cooking yield (A) of MP composite gels. The storage modulus G' (B) of OP-MP composite solutions subjected to heating (from 20 to 90 °C). Graph bars with different letter (a–c) represent significant ($P < 0.05$) difference. Effects of OP addition (0%~1%) on the protein solubilities (C) contributed by ionic bonds, hydrogen bonds, hydrophobic interactions, and disulfide bonds in MP gels.

network formation process (20–90 °C) (Han et al., 2022): (1) the process of protein pregelation (suwari, 20–40 °C), (2) the process of weakening of the protein gel network (modori, 40–45 °C), and (3) the process of strengthening the gel network structure (kamaboko, 45–90 °C). During the gel strengthening stage, the G′ of the OP-MP hybrid gels with 0.75% OP addition (4.09 Pa) was significantly ($P < 0.05$) greater than that of the pure protein gel (1.84 Pa) when the temperature increased to 75 °C (Fig. 2 (B)) and showed superior rheological properties to those of the pure MP gel. The rheological behavior of the OP-MP complex system demonstrated that the presence of OP increased the viscosity of the MP system. OP is of high molecular weight with a random-coil conformation, which makes it an effective rheological modifier even at low contents (Alba et al., 2021). An increase in the OP content caused a significant ($P < 0.05$) increase in viscosity and advanced the gelation and interaction between MPs (Zhou et al., 2021; Xu et al., 2017). It can be inferred from the above results that the macromolecular arrangement of the system could be produced by intermolecular interactions of OP-MP associations or OP self-association and MP self-association via hydrogen bonding and other interactions (Monteiro et al., 2013). The G′ of the OP-MP complex system decreased as the content of OP increased to more than 0.75%, which could be attributed to the excessive particle size of the composite system. The steric hindrance effect caused by excessive particle size hindered the interaction between proteins, making the protein structure loose, thus reducing the gel properties of the composite system (Li et al., 2019).

3.3. Effects of OP on the intermolecular forces of MPs

Intermolecular forces are essential for the MP gelation process. Since the MP is subjected to thermal gel treatment, the proportion of ionic bonds and hydrogen bonds is relatively small, and the high content of hydrophobic interactions and disulfide bonds are important crucial forces for sustaining the protein gel (Zhu et al., 2022). The addition of OP could significantly ($P < 0.05$) decrease the solubility of MP influenced by ionic bonds in the MP gels (Fig. 2 (C)), which indicated that the addition of a certain amount of OP might change the charge distribution in the electrostatic interactions between MP molecules (Zhou et al., 2021). Moreover, the influence of hydrogen bonds on the solubility of MP after the addition of OP was significantly ($P < 0.05$) greater than that of the control group, which was consistent with the WHC results (Fig. 2 (A)). The OP added to the MP attracted more water to the protein network due to the hydrophilicity of the OP, which increased the hydrogen bonding content of the MP (Mi et al., 2022). As shown in Fig. 2 (C), 0.25%~1% OP significantly ($P < 0.05$) promoted the formation of hydrophobic interactions between MPs, and the highest value was achieved when the addition amount of OP was 0.75%. The increase in the strength of the MP gel after the addition of OP (Fig. 2 (A)) may be related to the increase in the number of hydrophobic interactions between the MP molecules since the hydrophobic interactions could alter the texture of the gel (Zhou et al., 2021). The effect of disulfide bonds on the solubility of MP was dominated by intermolecular forces. Compared to the solubility of the control group, the solubility of MP, influenced by disulfide bonds between MPs, was considerably ($P < 0.05$) weaker with the addition of OP (0.25%~0.75%). The enhanced hydrophobic interactions between MPs caused MP aggregation, which may inhibit further cross-linking of MP through disulfide bonds (Kou et al., 2019). In addition, numerous investigations have demonstrated that during protein thermal gelation, sulfhydryl linkages are oxidized to create disulfide bonds (Mi et al., 2022). OP has antioxidant activity (Olawuyi and Lee, 2021) and can reduce the degree of protein oxidation, thereby inhibiting the formation of disulfide bonds. The results indicated that ionic bonds, hydrogen bonds, hydrophobic interactions, disulfide bonds and their interactions collectively affect the gel properties of MP, especially increasing hydrophobic interactions and decreasing disulfide bonds. The gel properties of MP are positively correlated with disulfide bonds and hydrophobic interactions (Han et al., 2022). The addition of OP

enhanced the gelling characteristics of the OP, indicating that the importance of noncovalent bonds exceeded that of covalent bonds.

3.4. Molecular interactions in OP-MP composites

Fourier transform infrared (FTIR) spectroscopy is an effective method for analyzing molecular structure and can reflect the functional groups and molecular structure information of samples (Chen et al., 2019). Fig. 3 (A) and Table 1 show the FTIR spectra and absorption peaks of OP, MP, and the OP-MP composite gels. As shown in Fig. 3 (A), OP had the characteristic infrared absorption peak of general polysaccharides. The absorption peak at approximately 1600 cm^{-1} was assigned to the stretching vibration peak of the C═O group, confirming the presence of uronic acids in the OP (Wu et al., 2020). The –CH vibration peak in the range of 1000–1200 cm^{-1} indicated that OP may contain a pyranose ring (Olawuyi and Lee, 2021). The 3200-3600 cm^{-1} region of the pure MP sample displayed strong and wide bands (Fig. 3 (A)), attributed to intermolecular H–bonded N–H and O–H stretching vibrations (Fan et al., 2017). The protein bands at approximately

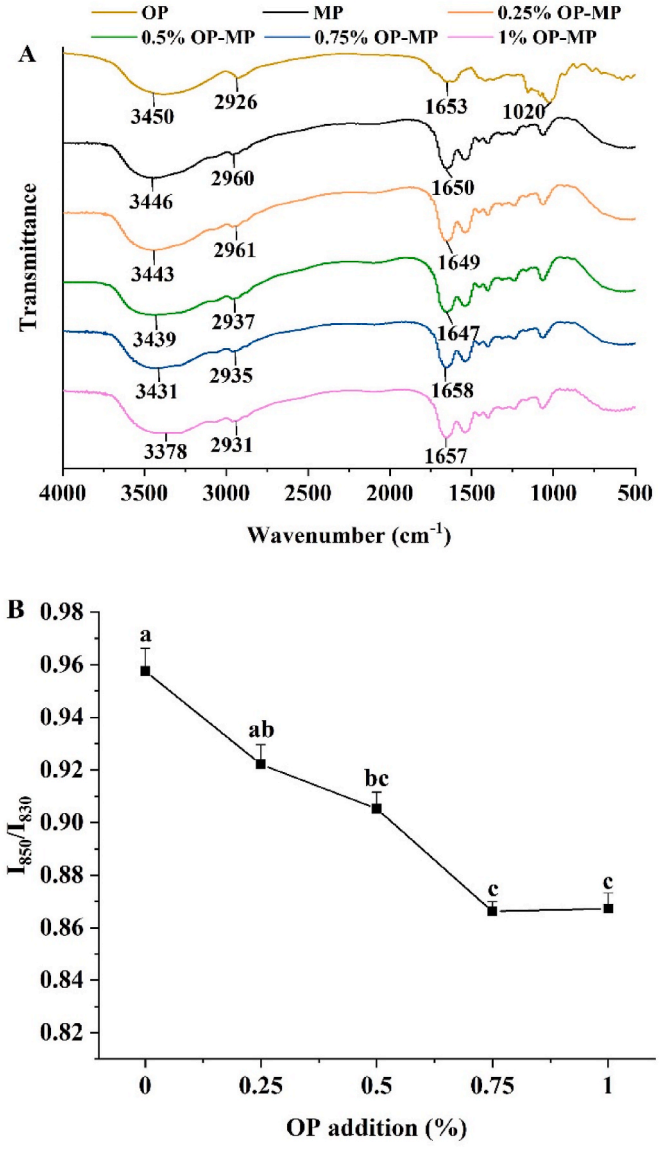

Fig. 3. Changes in FTIR (A) of OP, MP, OP-MP composite gels (0.25%~1% OP addition). Effect of OP addition (0%~1%) on the I_{850}/I_{830} intensity ratio (B) of MP in OP-MP composite gel. Graph bars with different letter (a–c) represent significant ($P < 0.05$) difference.

1600–1700 cm^{-1}, 1500-1600 cm^{-1} and 1200-1400 cm^{-1} are attributed to amide I (80% C═O stretch, 10% C–N stretch), amide II (60% N–H bend, 30% C–N stretch and 10% C–C stretch) and amide III (complex bands resulting from several coordinate displacements), respectively (Kaddour et al., 2008). The characteristic absorption peaks of OP and MP could be observed in the FTIR spectra of the OP-MP composites, and no new absorption peaks appeared, indicating that there was no chemical cross-linking between OP and MP. MP mainly interacts with OP through noncovalent interactions. As shown in Table 1, the O–H stretching vibration peaks of pure OP and pure MP were at 3449.33 and 3446.00, respectively. The peak intensity of the OP-MP composites increased, and the peak gradually shifted to a lower wavenumber as the OP increased, indicating an increase in the number of hydrogen bonding interactions in the composite system (Kou et al., 2019).

The microenvironment around the tyrosine (Tyr) residues can be observed at 830 cm^{-1} and 850 cm^{-1}, and the intensity ratio of I_{850}/I_{830} suggested the presence of hydrogen bonds in the phenolic hydroxyl groups (Kou et al., 2019). As shown in Fig. 3 (B), the intensity ratio of I_{850}/I_{830} was in the range of 0.8–1, and the Tyr residues were buried in the protein to participate in the formation of intermolecular/intramolecular hydrogen bonds (Han et al., 2022; Shi et al., 2022). With increasing OP content, the I_{850}/I_{830} ratio of the OP−MP mixed gels gradually decreased (Fig. 3 (B)), increasing Tyr burial and decreasing hydrophobicity (Zhou et al., 2021). Considering the large amount of galactose and rhamnose in the OP (Olawuyi and Lee, 2021), the hydroxyl groups of MP may compete with the OP for water molecules (Han et al., 2022), thereby reducing the number of hydrogen bonds between the MP and the water molecules. Furthermore, with increasing OP content, the number of hydrogen bonds between MP molecules decreased (Fig. 2 (C)). Consequently, integrant MP molecules bind to OP molecules through hydrogen bonds. The increase of hydrogen bonds may be due to the transformation of α-helix to other secondary structures, which was conducive to the formation of well-ordered gel structure (Zhang et al., 2020).

3.5. Effects of OP on the secondary structures of MP

Far-UV CD was utilized to assess protein conformation changes upon OP binding at Stages A (Fig. 4(A–C)) and B (Fig. 4(B–D)). The CD spectrum of the MP mainly had two negative peaks at 208 and 222 nm (Fig. 4(A and B)), indicating that the α-helix structure mainly existed due to the myosin tail having α-helix structure (Zhang et al., 2020). The content of the α-helix structure in the MP in Stage B was lower than that in Stage A (Fig. 4(C and D)), indicating that the unfolding of the MP was induced by heating (Xu et al., 2021). As the OP content increased from 0% to 1%, the β-sheet and β-turn contents increased and then decreased (Fig. 4 (D)). The content of the α-helix structure (19.5%) was the lowest ($P < 0.05$) when the addition amount of OP was 0.75%, while the content of β-sheets (27.6%) was the highest ($P < 0.05$) (Fig. 4 (D)). OP promoted the transformation of the secondary structure of MP from α-helix to β-sheet because OP promoted the rearrangement of hydrogen bonds in MP molecules (Xu et al., 2021). Previous studies have shown that the increase in β-sheet content with decreasing α-helix content is mostly related to the formation of a stable protein backbone and an orderly gel structure (Li et al., 2019). OP promoted the unfolding of protein structures and the exposure of hydrophobic groups during heating, leading to the mutual conversion of protein secondary structures and enhancing protein gel development, resulting in a dense three-dimensional network structure and high gel strength (Zhang et al., 2020).

3.6. Effects of OP on the tertiary structures of MP

The intrinsic tryptophan fluorescence of proteins is easily affected by the microenvironment around the protein, and protein conformational changes are frequently characterized by fluorescence intensity (FI) (Cao

Table 1
The absorption peaks of OP and OP-MP composites with different addition of OP.

Absorption peak	Wave number (cm^{-1})	Samples					
		OP	MP	0.25% OP-MP	0.5% OP-MP	0.75% OP-MP	1% OP-MP
Associated O–H stretching vibration peak	3600–3000	3449.33 ± 3.06^{a}	3446.00 ± 5.00^{ab}	3439.00 ± 5.29^{ab}	3433.33 ± 8.14^{bc}	3423.37 ± 8.74^{c}	3364.33 ± 12.34^{d}
C–H stretching vibration peak	3000–2800	2924.33 ± 6.66^{c}	2958.67 ± 4.16^{a}	2959.67 ± 5.51^{a}	2936.49 ± 5.38^{b}	2935.00 ± 5.00^{b}	2932.00 ± 5.57^{bc}
C═O peak	1700–1500	1653.33 ± 4.51^{ab}	1649.00 ± 5.57^{ab}	1648.00 ± 2.65^{b}	1647.13 ± 6.51^{b}	1658.33 ± 3.51^{a}	1657.49 ± 2.52^{a}
O–H bending vibration peak	1500–1400	1417.91 ± 1.36^{b}	1422.41 ± 2.50^{b}	1455.65 ± 5.13^{a}	1455.51 ± 0.68^{a}	1456.16 ± 6.01^{a}	1455.49 ± 2.17^{a}
C–H angle vibration peak	1400–1200	1280.02 ± 54.55^{a}	1241.32 ± 7.51^{b}	1240.98 ± 1.71^{b}	1241.21 ± 1.70^{b}	1240.66 ± 3.51^{b}	1238.52 ± 2.50^{b}
C–H bending vibration peak	1200–600	928.80 ± 4.43^{c}	936.60 ± 1.22^{b}	933.63 ± 1.19^{bc}	936.45 ± 5.02^{b}	932.30 ± 2.07^{bc}	946.61 ± 4.14^{a}

Mean values with different letters (a–c) of each row differ significantly ($P < 0.05$).

et al., 2021). The protein was shown to be folded by the high FI, where tryptophan residues are typically found in the core (a hydrophobic environment) (Li et al., 2019). As shown in Fig. 4 (E), the greatest ($P < 0.05$) FI was in the control group (pure MP), and the FI_{max} gradually decreased with increasing OP, indicating the occurrence of fluorescence quenching. The FI of the OP-MP mixture in the Stage B group increased at 0.25% OP before declining at 0.5%–0.75% OP addition and then increased slightly, as displayed in Fig. 4 (F). The fluorescence intensities of the Stage A and B groups reached their lowest values when the amount of added OP was 1% and 0.75%, respectively, which may be due to the different heating conditions and the synergistic effect of OP. The conformation of the MP changes after heat treatment, resulting in changes in the microscopic chemical environment of the protein molecules (Li et al., 2022). Gao et al. (2022) also reported that 0.75% konjac glucomannan caused MP to have exposed tryptophan residues. FI in MP decreased with the addition of OP, indicating protein unfolding and potential interactions between OP and tryptophan residues (Yuennan et al., 2014). When the protein is partially or completely unfolded, the tryptophan residues are in a hydrophilic environment, resulting in a reduction in FI, which is a marker of the expansion of the protein tertiary structure (Gao et al., 2022). The unfolding of proteins is more likely to expose reactive groups (especially hydrophobic groups), which is conducive to enhancing hydrophobic interactions, hydrogen bonds and electrostatic interactions. This phenomenon is beneficial for strengthening the network between protein molecules and promoting the formation of irreversible gels (Li et al., 2019). The characteristics of the gels consequently improved with moderate OP addition.

3.7. Effects of OP on the microstructure of the MP gels

CLSM was used to observe the microstructures of the OP-MP combinations, as shown in Fig. 5(A–E, a-e). To confirm the distribution of each component in the OP−MP system, multiple fluorescent dyeing techniques were employed. The OP phase was stained green by Calcofluor White, and the MP phase was stained red by Fast Green. Yellow shows the mixing of the MP and OP. When the added OP content was 0%–0.25% (Fig. 5(A and B)), the MP and OP at Stage A showed a homogeneous distribution of tiny particles. Increasing the OP content gradually increased the degree of MP aggregation, and larger protein particles could be observed, consistent with the particle size results (Fig. 1 (B)). The protein network matrix might be filled with a small portion of OP (0.5%–1%) (Fig. 5 (C, D, and E)). The proteins treated with Stage B formed larger aggregates than those treated with Stage A due to the higher temperature of the heating treatment. MP monomers or oligomers crosslink and aggregate at different speeds depending on the temperature. Increasing temperatures promote covalent and hydrophobic interactions, which cause MPs to unfold and produce larger particles more quickly (Li et al., 2022). OP was dispersed outside the protein-gathering network at a 0.25% content (Fig. 5 (b)). In the content range of 0.5%–1% (Fig. 5 (c, d, and e)), OP could evenly fill the MP network and interact with MP molecules to influence the structure of the MP. After the addition of OP (0%–0.75%), the number of small protein clusters decreased, the gap between small protein clusters narrowed, and the clusters gradually gathered into larger protein clusters (Fig. 5 (a, b, c, and d)), which aided in enhancing the WHC and gel strength (Fig. 2 (A)). As shown in Fig. 5 (a) and 5 (d), compared with the average protein cluster size of the pure MP solution (54.7 μm), that of the MP solution with 0.75% OP (201 μm) increased significantly ($P < 0.05$). Similarly, Xu et al. (2019a) reported that the addition of OP was apparently beneficial for increasing protein clusters because OP is very viscous.

The microstructure of the MP gels with different OP additions is presented in Fig. 5(F–J). The gel network of the MPs in the control group was segmented by numerous “water channels”, forming a coarse and porous gel network. The original moisture that the MP had absorbed was released because of the denaturation of MP molecules during the creation of the heat-induced gel, which eventually produced a significant number of moisture holes or associated moisture channels in the gel network structure. The stability of the three-dimensional network was disrupted by these interconnected moisture channels, which divided the structure of the network into many cluster-shaped sections (Han et al., 2022). With increasing OP content (0.25%–0.75%), the pore distribution of the OP-MP composite gel network became more uniform and had smaller pores (Fig. 5 (G, H, and I)), which was conducive to the formation of a dense protein network structure. According to the results, the addition of OP (0.25%–0.75%) may reduce random moisture leakage in the MP gel network, improve the WHC of the OP-MP gels, and form dense gel networks, thereby reducing the cooking loss of the gels (Shi et al., 2022). In particular, the presence of 0.75% OP promoted cross-linking between protein molecules, leading to the uniform distribution of independent water cavities in the protein network (Fig. 5 (I)). The higher WHC of the gel might be attributed to the increased hydrophobic interactions between the MPs, which narrowed the water channels and created a homogenous structure (Sun et al., 2024). This may be because OP functions as a powerful binder between MP molecules through hydrogen bonds, reducing the loss of water in the gel network and thereby improving its stability.

3.8. Molecular docking

To investigate the interaction between MP and OP, the MHC, which can create gels in the same way as intact myosin can (Shi et al., 2022), was used as a receptor. Fig. 6 (A) depicts the anticipated 3D structure of the MHC protein. Galactose and rhamnose are the two main monosaccharides in OP, with molar ratios of 18.3 and 5.5, respectively (Liu et al., 2018). The galactose and rhamnose were chosen as small-molecule ligands. The molecular interactions between the MHC

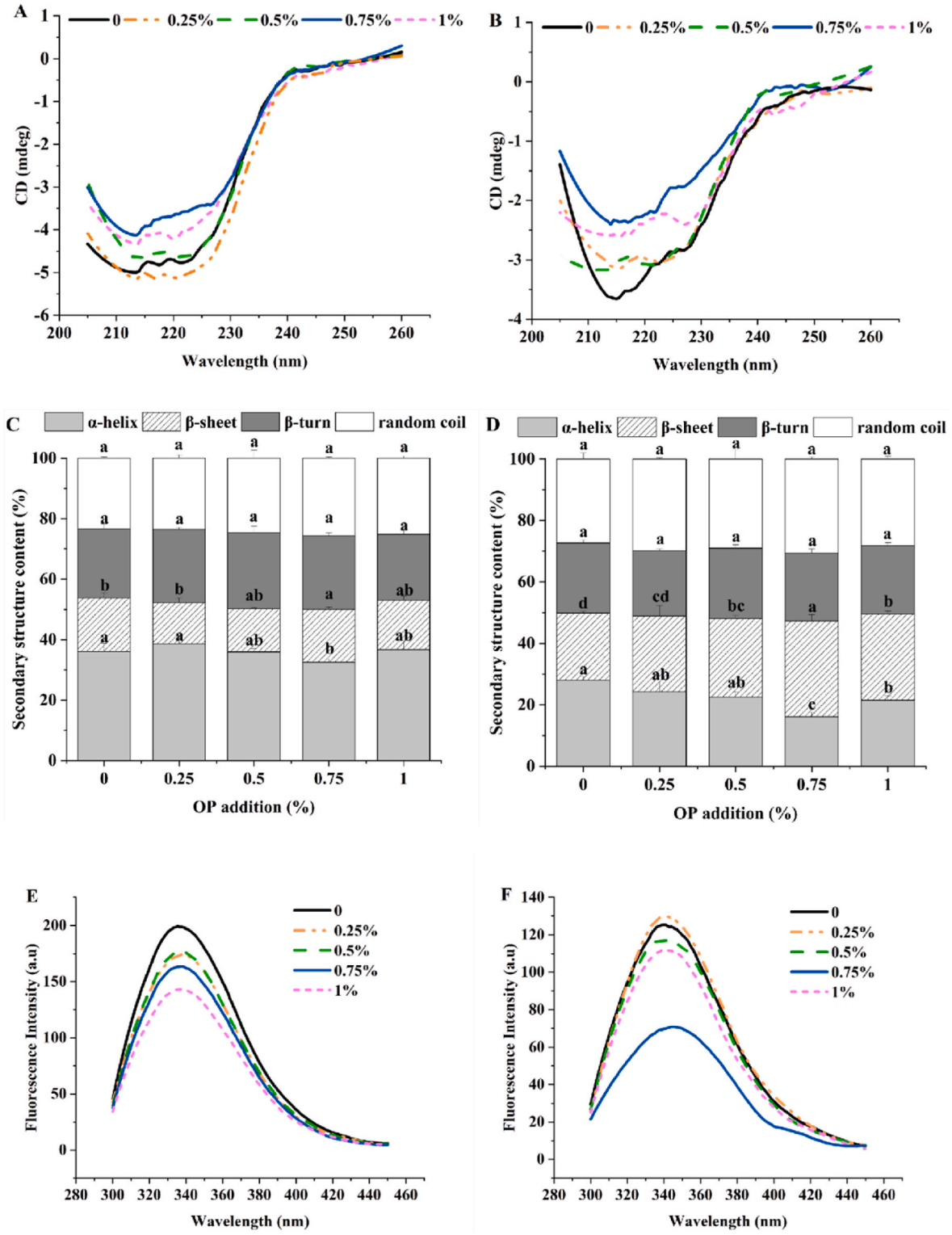

Fig. 4. Effects of OP addition (0%~1%) on the CD spectra of MP treated with Stage A (A) and B (B) heating. Effects of OP addition (0%~1%) on the protein secondary structure content of MP treated with Stages A (C) and B (D) heating. Graph bars with different letter (a–e) represent significant ($P < 0.05$) difference. Effects of OP addition (0%~1%) on the intrinsic tryptophan fluorescence of MP treated with Stages A (E) and B (F) heating.

protein and galactose/rhamnose determined via computer-aided docking are illustrated in Fig. 6 (B, C, and D) and Fig. 6 (E, F, and G). The binding energies of the MHC protein for galactose and rhamnose were −5.55 and −5.4 kcal/mol, respectively, indicating that the ability of the MHC protein to bind to galactose was comparable to that of rhamnose. The interaction between the protein and the two monosaccharides occurred spontaneously, according to the negative value of the binding energy of myosin-galactose/rhamnose, with lower values indicating simpler binding (Wang et al., 2022).

Galactose and rhamnose were introduced into the myosin active region, which interacted with a few amino acids (Fig. 6(B–E)), and altered the hydrophobic environment both internally and externally of

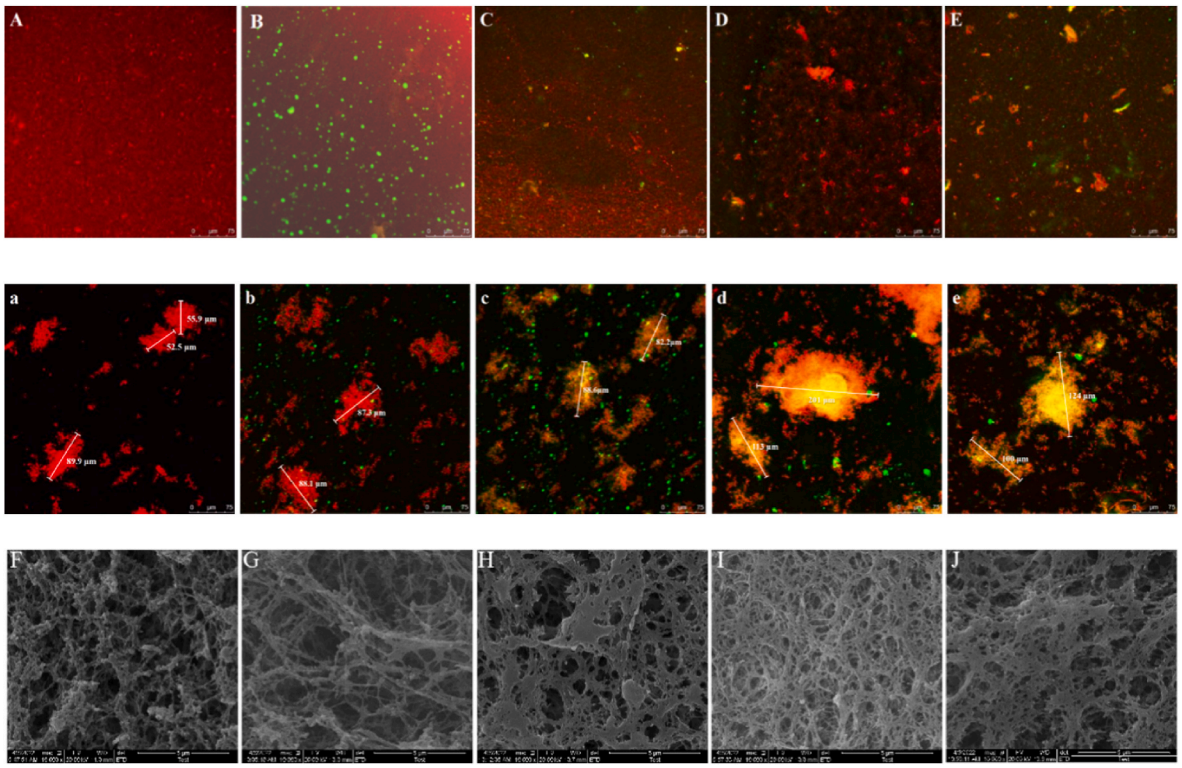

Fig. 5. Effects of OP addition (0%~1%) on the CLSM of MP treated with Stages A (A–E) and B (a–e) heating. SEM micrographs at 10,000× magnification of MP gels with OP addition (0%~1%) (F–J).

myosin. The results showed that galactose and rhamnose mostly engaged in hydrophobic and hydrogen bonding interactions with myosin, which was related to the fluorescence quenching of MP with an OP addition (Fig. 4(E and F)) (Zhu et al., 2022). Lysine, isoleucine, and threonine residues are the major binding sites for the two monosaccharides and MHC proteins, functioning by adhering firmly to the exterior or interior cavities of protein-peptide chains (Zhou et al., 2021). Galactose established hydrogen bonds with Ala182, Lys184, Ile464, and Thr185 in myosin (Fig. 6 (D)). According to Fig. 6 (G), hydrogen bonds accounted for the majority of the interactions between the Lys184, Ile464, Thr185, Gly181, Ser 243, Ser 244, and Asn240 residues in myosin and rhamnose. Moreover, there was a hydrophobic interaction between the rhamnose and Val186 residues of myosin. An appropriate dose of OP promoted MP aggregation by promoting hydrophobic interactions between the hydrophobic amino acids of MP. Based on the results of molecular docking, the two monosaccharides with higher contents in the OP mainly bind to myosin through hydrogen bonds, which is consistent with the results of molecular interactions in OP-MP composites (Fig. 3(A and B)). OP can react with amino acid residues of MP and may disturb the conformation of MP, thus promoting MP aggregation and enhancing the gel-forming capabilities of MP. The results of the present study may help to elucidate the interactions between polysaccharides and proteins. However, due to the large molecular weight and complex structure of polysaccharides, the interactions between polysaccharides and MPs may be more complicated. Further experiments and newer analytical techniques are needed to investigate this issue.

4. Conclusion

The findings demonstrated that the addition of 0.75% OP had the greatest ($P < 0.05$) effect on enhancing the gel characteristics of MP. The gel strength (21.79 g × mm) and WHC (51.01%) of the protein gel peaked at 0.75% OP content. OP could uniformly fill in around the protein, thus interacting with MP. The interaction between OP and MP interfered with the molecular rearrangement of MP during heating, which increased the β-sheet content and enhanced the interactions between MP. The addition of OP induced the exposure of more hydrophobic groups on the MP, which enhanced the hydrophobic interactions between the MP molecules. The hydrogen bonds between MP molecules were strengthened by the addition of OP, and the hydroxyl groups of OP could form hydrogen bonds with the hydroxyl groups of MP. There was a more compact and uniform gel network structure and a reduction of the pores inside the composite gel with 0.75% OP. An increase in the number of hydrophobic interactions between MP molecules promoted the aggregation of MP and eventually improved the gel properties of the OP–MP composite system. An excess of OP might bind to the hydrophobic amino acid residues exposed during the heating of MP through hydrogen bonds, thereby reducing the hydrophobic interactions between the MP and ultimately leading to a decrease in the gel properties of the MP. This study provides an extensive resource for developing surimi products and broadening the application of OP in the surimi industry. However, the specific and safe levels of OP to be added to surimi and surimi products need to be further explored.

CRediT authorship contribution statement

Xin Wang: Writing – original draft, Data curation, Formal analysis, Methodology, Investigation. **Mengzhe Li:** Methodology. **Tong Shi:** Supervision, Conceptualization, Writing – review & editing, Funding acquisition. **Abdul Razak Monto:** Writing – review & editing. **Li Yuan:** Supervision, Conceptualization. **Wengang Jin:** Methodology. **Ruichang Gao:** Conceptualization, Funding acquisition, Project administration.

Declaration of competing interest

The authors declare that they have no known competing financial

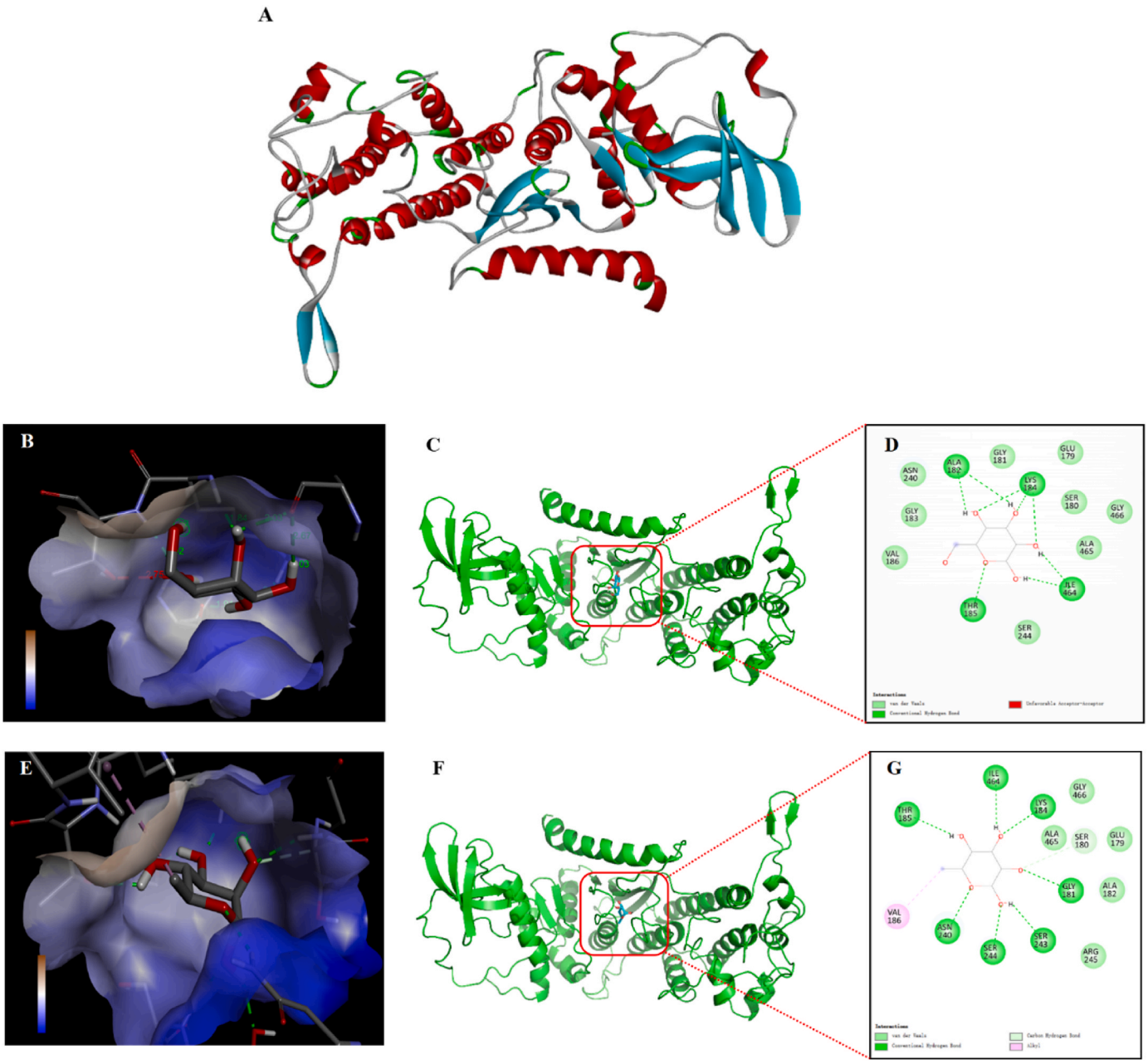

Fig. 6. Docking results of the myosin-galactose/rhamnose system. The predicted 3D structure with the highest score of *Aristichthys nobilis* MHC (A). 3D docking diagram of MHC and galactose (B) and rhamnose (E), showing the hydrophobic docking surface, where taupe represents hydrophobicity, and blue denotes hydrophilia. 3D representation of the interaction of MHC and galactose (C) and rhamnose (F). 2D docking diagram of MHC and galactose (D) and rhamnose (G) in which the color of the circles was determined by the type of interaction. (For interpretation of the references to color in this figure legend, the reader is referred to the Web version of this article.)

interests or personal relationships that could have appeared to influence the work reported in this paper.

Data availability

Data will be made available on request.

Acknowledgments

This work was supported by the National Natural Science Foundation of China (U20A2067, 32202090), the Natural Science Foundation of Jiangsu Province (BK20220520), the Postdoctoral Research Foundation of China (2022M721389).

References

Alba, K., Nguyen, P.T.M., Kontogiorgos, V., 2021. Sustainable polysaccharides from Malvaceae family: structure and functionality. Food Hydrocolloids 118, 106749. https://doi.org/10.1016/j.foodhyd.2021.106749.

Cao, Y.G., Li, B.L., Fan, X., Wang, J.K., Zhu, Z.B., Huang, J.R., Xiong, Y.L., 2021. Synergistic recovery and enhancement of gelling properties of oxidatively damaged myofibrillar protein by L-lysine and transglutaminase. Food Chem. 358, 129860 https://doi.org/10.1016/j.foodchem.2021.129860.

Chen, Y.X., Chen, J.C., Chang, C., Chen, J., Cao, F.W., Zhao, J.W., Zheng, Y.F., Zhu, J.J., 2019. Physicochemical and functional properties of proteins extracted from three microalgal species. Food Hydrocolloids 96, 510–517. https://doi.org/10.1016/j.foodhyd.2019.05.025.

Fan, M.C., Hu, T., Zhao, S.M., Xiong, S.B., Xie, J., Huang, Q.L., 2017. Gel characteristics and microstructure of fish myofibrillar protein/cassava starch composites. Food Chem. 218, 221–230. https://doi.org/10.1016/j.foodchem.2016.09.068.

Gao, Y.F., Luo, C., Zhang, J.Y., Wei, H.J., Zan, L.S., Zhu, J., 2022. Konjac glucomannan improves the gel properties of low salt myofibrillar protein through modifying protein conformation. Food Chem. 393, 133400 https://doi.org/10.1016/j.foodchem.2022.133400.

Gonzalez, A., Barrera, G.N., Galimberti, P.I., Ribotta, P.D., Alvarez Igarzabal, C.I., 2019. Development of edible films prepared by soy protein and the galactomannan fraction extracted from Gleditsia triacanthos (Fabaceae) seed. Food Hydrocoll. 97, 105227. https://doi.org/10.1016/j.foodhyd.2019.105227.

Han, K.Y., Li, S.S., Yang, Y.L., Feng, X., Tang, X.Z., Chen, Y.M., 2022. Mechanisms of inulin addition affecting the properties of chicken myofibrillar protein gel. Food Hydrocolloids 131, 107843. https://doi.org/10.1016/j.foodhyd.2022.107843.

Kaddour, A.A., Mondet, M., Cuq, B., 2008. Description of chemical changes implied during bread dough mixing by FT-ATR mid-infrared spectroscopy. Cereal Chem. 85 (5), 673–678. https://doi.org/10.1094/cchem-85-5-0673.

Kou, X.R., Luo, D.L., Zhang, K.Y., Xu, W., Li, X., Xu, B.C., Li, P.Y., Han, S.H., Liu, J., 2019. Textural and staling characteristics of steamed bread prepared from soft flour added with inulin. Food Chem. 301, 125272 https://doi.org/10.1016/j.foodchem.2019.125272.

Le, X.T., Rioux, L.E., Turgeon, S.L., 2017. Formation and functional properties of protein-polysaccharide electrostatic hydrogels in comparison to protein or polysaccharide hydrogels. Adv. Colloid Interface Sci. 239, 127–135. https://doi.org/10.1016/j.cis.2016.04.006.

Li, F.F., Wang, B., Liu, Q., Chen, Q., Zhang, H.W., Xia, X.F., Kong, B.H., 2019a. Changes in myofibrillar protein gel quality of porcine *longissimus* muscle induced by its stuctural modification under different thawing methods. Meat Sci. 147, 108–115. https://doi.org/10.1016/j.meatsci.2018.09.003.

Li, M.Z., Shi, T., Wang, X., Bao, Y.L., Xiong, Z.Y., Monto, A.R., Yuan, L., Gao, R.C., 2022a. Plasma-activated water promoted the aggregation of *Aristichthys nobilis* myofibrillar protein and the effects on gelation properties. Curr. Res. Food Sci. 5, 1616–1624. https://doi.org/10.1016/j.crfs.2022.09.003.

Li, X.X., Fan, M.C., Huang, Q.L., Zhao, S.M., Xiong, S.B., Yin, T., Zhang, B.J., 2022b. Effect of micro- and nano-starch on the gel properties, microstructure and water mobility of myofibrillar protein from grass carp. Food Chem. 366, 130579 https://doi.org/10.1016/j.foodchem.2021.130579.

Li, Z.Y., Wang, J.Y., Zheng, B.D., Guo, Z.B., 2019b. Effects of high pressure processing on gelation properties and molecular forces of myosin containing deacetylated konjac glucomannan. Food Chem. 291, 117–125. https://doi.org/10.1016/j.foodchem.2019.03.146.

Liu, J., Zhao, Y.P., Wu, Q.X., John, A., Jiang, Y.M., Yang, J.L., Liu, H.L., Yang, B., 2018. Structure characterisation of polysaccharides in vegetable "okra" and evaluation of hypoglycemic activity. Food Chem. 242, 211–216. https://doi.org/10.1016/j.foodchem.2017.09.051.

Ma, W.H., Yang, Q., Fan, X., Yao, X.Q., Kuang, J.W., Min, C., Cao, Y.G., Huang, J.R., 2022. Modification of myofibrillar protein gelation under oxidative stress using combined inulin and glutathione. Food Chemistry-X 14, 100318. https://doi.org/10.1016/j.fochx.2022.100318.

Mi, J., Ni, W., Huang, P., Hong, J.X., Jia, R., Deng, S.G., Yu, X.X., Wei, H.M., Yang, W.G., 2022. Effect of acetylated distarch adipate on the physicochemical characteristics and structure of shrimp (Penaeus vannamei) myofibrillar protein. Food Chem. 373, 131530 https://doi.org/10.1016/j.foodchem.2021.131530.

Monteiro, S.R., Rebelo, S., da Cruz e Silva, O.A.B., Lopes-da-Silva, J.A., 2013. The influence of galactomannans with different amount of galactose side chains on the gelation of soy proteins at neutral pH. Food Hydrocolloids 33 (2), 349–360. https://doi.org/10.1016/j.foodhyd.2013.04.012.

Nagae, M., Yamaguchi, Y., 2014. Three-dimensional structural aspects of protein-polysaccharide interactions. Int. J. Mol. Sci. 15 (3), 3768–3783. https://doi.org/10.3390/ijms15033768.

Olawuyi, I.F., Lee, W.Y., 2021. Structural characterization, functional properties and antioxidant activities of polysaccharide extract obtained from okra leaves (*Abelmoschus esculentus*). Food Chem. 354, 129437 https://doi.org/10.1016/j.foodchem.2021.129437.

Pirsa, S., Hafezi, K., 2023. Hydrocolloids: structure, preparation method, and application in food industry. Food Chem. 399, 133967 https://doi.org/10.1016/j.foodchem.2022.133967.

Shi, T., Wang, X., Li, M.Z., Xiong, Z.Y., McClements, D.J., Bao, Y.L., Yuan, L., Gao, R.C., 2022. Mechanism of low-salt surimi gelation induced by microwave heating combined with L-arginine and transglutaminase: on the basis of molecular docking between L-arginine and myosin heavy chain. Food Chem. 391, 133184 https://doi.org/10.1016/j.foodchem.2022.133184.

Shi, T., Xiong, Z.Y., Liu, H.J., Jin, W.G., Mu, J.L., Yuan, L., Sun, Q.C., McClements, D.J., Gao, R.C., 2021. Ameliorative effects of L-arginine on heat-induced phase separation of *Aristichthys nobilis* myosin are associated with the absence of ordered secondary structures of myosin. Food Res. Int. 141, 110154 https://doi.org/10.1016/j.foodres.2021.110154.

Shi, X.J., Zou, H.N., Sun, S., Lu, Z.R., Zhang, T.Y., Gao, J.Z., Yu, C.P., 2019. Application of high-pressure homogenization for improving the physicochemical, functional and rheological properties of myofibrillar protein. Int. J. Biol. Macromol. 138, 425–432. https://doi.org/10.1016/j.ijbiomac.2019.07.110.

Sun, X.Y., Li, Q., Ding, N., Liang, S.J., Mubango, E., Zheng, Y.Y., Yu, Q.Y., Dai, R.T., Hong, H., 2024. Cryoprotective effect of fistular onion stalk polysaccharide on frozen surimi derived from bighead carp: physicochemical properties and gel quality during storage. Food Hydrocolloids 148, 109404. https://doi.org/10.1016/j.foodhyd.2023.109404.

Wang, H.T., Zhang, H.W., Liu, Q., Xia, X.F., Chen, Q., Kong, B.H., 2022. Exploration of interaction between porcine myofibrillar proteins and selected ketones by GC-MS, multiple spectroscopy, and molecular docking approaches. Food Res. Int. 160, 111624 https://doi.org/10.1016/j.foodres.2022.111624.

Wu, D.M., Zheng, J.Q., Hu, W.W., Zheng, X.L., He, Q.J., Linhardt, R.J., Ye, X.Q., Chen, S.G., Chen, S.G., 2020. Structure-activity relationship of Citrus segment membrane RG-I pectin against Galectin-3: the galactan is not the only important factor. Carbohydr. Polym. 245, 116526 https://doi.org/10.1016/j.carbpol.2020.116526.

Xu, K., Guo, M.M., Du, J.H., 2017. Molecular characteristics and rheological properties of water-extractable polysaccharides derived from okra (*Abelmoschus esculentus L.*). Int. J. Food Prop. 20, S899–S909. https://doi.org/10.1080/10942912.2017.1315594.

Xu, K., Guo, M.M., Du, J.H., Zhang, Z.H., 2019a. Okra polysaccharide: effect on the texture and microstructure of set yoghurt as a new natural stabilizer. Int. J. Biol. Macromol. 133, 117–126. https://doi.org/10.1016/j.ijbiomac.2019.04.035.

Xu, K., Zhao, Z.T., Guo, M.M., Du, J.H., 2019b. Conjugation between okra polysaccharide and lactoferrin and its inhibition effect on thermal aggregation of lactoferrin at neutral pH. LWT–Food Sci. Technol. 107, 125–131. https://doi.org/10.1016/j.lwt.2019.02.082.

Xu, Y.X., Yin, Y.M., Wang, R., Zhao, H.L., Li, X.P., Yi, S.M., Li, J.R., Xie, J.C., 2021. Effect of deacetylated konjac glucomannan on heat-induced structural changes and flavor binding ability of fish myosin. Food Chem. 365, 130540 https://doi.org/10.1016/j.foodchem.2021.130540.

You, G., Niu, G.G., Zhou, X.Y., Gao, K., Liu, X.L., 2023. Interactions of heat-induced myosin with hsian-tsao polysaccharide to affect the fishy odor adsorption capacity. Food Hydrocolloids 136, 108282. https://doi.org/10.1016/j.foodhyd.2022.108282.

Yuennan, P., Sajjaanantakul, T., Goff, H.D., 2014. Effect of okra cell wall and polysaccharide on physical properties and stability of ice cream. J. Food Sci. 79 (8), E1522–E1527. https://doi.org/10.1111/1750-3841.12539.

Zhang, S.J., Zhang, L.Z., Yin, T., You, J., Liu, R., Wang, L., Huang, Q.L., Wamg, W.S., Ma, H., 2023. Exploring the versatility of carbohydrates in surimi and surimi products: novel applications and future perspectives. J. Sci. Food Agric. 104 (4), 1874–1883. https://doi.org/10.1002/jsfa.13081.

Zhang, Y.M., Dong, M., Zhang, X.Y., Hu, Y.J., Han, M.Y., Xu, X.L., Zhou, G.H., 2020. Effects of inulin on the gel properties and molecular structure of porcine myosin: a underlying mechanisms study. Food Hydrocolloids 108, 105974. https://doi.org/10.1016/j.foodhyd.2020.105974.

Zhou, Y., Dai, H.J., Ma, L., Yu, Y., Zhu, H.K., Wang, H.X., Zhang, Y.H., 2021a. Effect and mechanism of psyllium husk (*Plantago ovata*) on myofibrillar protein gelation. LWT–Food Sci. Technol. 138, 110651 https://doi.org/10.1016/j.lwt.2020.110651.

Zhou, Z.Q., Xu, Q.D., Chen, L., Chen, N., Gao, H.X., Sun, Q., Zeng, W.C., 2021b. Interaction and action mechanism of quercetin and myofibrillar protein and its effects on the quality of cured meat. J. Food Process. Preserv. 45 (12), e16020 https://doi.org/10.1111/jfpp.16020.

Zhu, N., Zang, M.W., Wang, S.W., Zhang, S.L., Zhao, B., Liu, M., Qiao, X., 2022. Modulating the structure of lamb myofibrillar protein gel influenced by psyllium husk powder at different NaCl contents: effect of intermolecular interactions. Food Chem. 397, 133852 https://doi.org/10.1016/j.foodchem.2022.133852.

Zhuang, X.B., Wang, L.J., Jiang, X.P., Chen, Y.J., Zhou, G.H., 2021. Insight into the mechanism of myofibrillar protein gel influenced by konjac glucomannan: moisture stability and phase separation behavior. Food Chem. 339, 127941 https://doi.org/10.1016/j.foodchem.2020.127941.